Acta Biomaterialia 75 (2018) 263–278

Contents lists available at ScienceDirect

Acta Biomaterialia

journal homepage: www.elsevier.com/locate/actabiomat

Full length article

Location-dependent correlation between tissue structure and the mechanical behaviour of the urinary bladder

Enrique Morales-Orcajo [a], Tobias Siebert [b], Markus Böl [a,*]

[a] Institute of Solid Mechanics, Technische Universität Braunschweig, Braunschweig D-38106, Germany
[b] Institute of Sport and Motion Science, University of Stuttgart, Stuttgart D-70569, Germany

ARTICLE INFO

Article history:
Received 5 January 2018
Received in revised form 4 May 2018
Accepted 9 May 2018
Available online 26 May 2018

Keywords:
Urinary bladder wall
Biaxial tension testing
Tissue composition
Microstructure
Smooth muscle
Tissue staining

ABSTRACT

The mechanical properties of the urinary bladder wall are important to understand its filling-voiding cycle in health and disease. However, much remains unknown about its mechanical properties, especially regarding regional heterogeneities and wall microstructure. The present study aimed to assess the regional differences in the mechanical properties and microstructure of the urinary bladder wall. Ninety ($n = 90$) samples of porcine urinary bladder wall (ten samples from nine different locations) were mechanically and histologically analysed. Half of the samples ($n = 45$) were equibiaxially tested within physiological conditions, and the other half, matching the sample location of the mechanical tests, was frozen, cryosectioned, and stained with Picro-Sirius red to differentiate smooth muscle cells, extracellular matrix, and fat. The bladder wall shows a non-linear stress-stretch relationship with hysteresis and softening effects. Regional differences were found in the mechanical response and in the microstructure. The trigone region presents higher peak stresses and thinner muscularis layer compared to the rest of the bladder. Furthermore, the ventral side of the bladder presents anisotropic characteristics, whereas the dorsal side features perfect isotropic behaviour. This response matches the smooth muscle fibre bundle orientation within the tunica muscularis. This layer, comprising approximately 78% of the wall thickness, is composed of two fibre bundle arrangements that are cross-oriented, one with respect to the other, varying the angle between them across the organ. That is, the ventral side presents a 60°/120° cross-orientation structure, while the muscle bundles were oriented perpendicular in the dorsal side.

Statement of Significance

In the present study, we demonstrate that the mechanical properties and the microstructure of the urinary bladder wall are heterogeneous across the organ. The mechanical properties and the microstructure of the urinary bladder wall within nine specific locations matching explicitly the mechanical and structural variations have been examined. On the one hand, the results of this study contribute to the understanding of bladder mechanics and thus to their functional understanding of bladder filling and voiding. On the other hand, they are relevant to the fields of constitutive formulation of bladder tissue, whole bladder mechanics, and bladder-derived scaffolds i.e., tissue-engineering grafts.

1. Introduction

The urinary bladder (UB), as a musculomembranous hollow organ, is accountable for two main cyclic functions: to temporally store urine at a low-pressure level (passive phase) and to control micturition (active phase). During the passive phase of filling, the bladder is exposed to enormous deformations, thereby keeping the internal pressure nearly constant until reaching its maximal capacity [66]. Dependent on the species, the process of bladder filling takes several hours, whereas micturition occurs within a few seconds. Consequently, the passive filling phase is frequently assumed to take place under quasi-static conditions. Interestingly, even if the bladder bears in its maximum loaded configuration enormous deformations, its shape returns completely back to its reference state. This capability is due to the microstructure of the UB wall, consisting of several layers (from the inside out): tunica mucosa, tunica submucosa, tunica muscularis, and tunica serosa. For more details on the microstructure, the interested reader is referred to Seydewitz et al. [58].

* Corresponding author.
E-mail address: m.boel@tu-bs.de (M. Böl).

https://doi.org/10.1016/j.actbio.2018.05.014
1742-7061/

To understand the load transfer mechanisms inside the UB wall during the passive phase, mechanical experiments in combination with detailed information on its microstructural constituents, i.e elastin, collagen, and smooth muscle (SM) cells, as well as their distributions are essential. Furthermore, these data are suitable for three-dimensional continuum mechanical-based models [58], which in turn could help in understanding the load transfer mechanisms inside the UB wall, as some scenarios are feasibly computational but cannot be realised experimentally.

Two types of mechanical experiments can be found in the literature. The first type addresses the characterisation of the mechanical behaviour of whole bladders, and the second considers dissected UB wall tissue strips, to be tested uniaxially or biaxially, to determine appropriate material characteristics. To study the mechanical functions of the bladder, observations on whole bladders during the filling and micturition cycles are indispensable. Consequently, cystometry, a urodynamic testing technique, is the preferred method [2,65,68,55,19,38,49,63,7,34,54]. Experimental studies in this field range from analyses using classical cystometry to more advanced methods where the cystometrical setup is combined, e.g. with imaging techniques, such as ultrasonography. The main advantage of this testing technique is the fact that it can be realised *in vivo* and non-invasively. With this technique, it is possible to study the mechanical functions of healthy and diseased UBs, which enables cystometry to be applied daily in clinical practice.

However, besides the aforementioned advantage of cystometry, its disadvantage is that questions concerning location-dependent mechanisms of structural characteristics remain unanswered. For the determination of these location-dependent characteristics, experiments on dissected tissue strips are of high interest. Two types of experiments on tissue strips can be found. While uniaxial tension experiments have been frequently realised (e.g. [23,55,18,11,37,41,72,5,48,42,58]), the number of biaxial tension studies is significantly smaller [6,28,45,47,40,26,64,69,14]. Generally, uniaxial experiments can be realised much more easily than biaxial tension experiments. In doing so, a rectangular tissue strip is fixed into two mounting devices that are pulled apart from each other. Meanwhile, an optical system records the distance changes in markers applied on top of the specimen. Depending on the mounting device, axial or uniaxial deformation can be achieved. However, when determining the mechanical characteristics of anisotropic materials, single uniaxial tests are insufficient, and several, orientation-dependent uniaxial tests are needed to identify the anisotropic behaviour. Even if this seems logical from a mechanical point of view, only five of the aforementioned uniaxial studies realised orientation-dependent experiments [37,41,72,48,58]. Furthermore, for a more comprehensive understanding of bladder mechanics, especially in relation to its function, knowledge of location-dependent characteristics is of particular importance. Within the studies found on uniaxial experiments, only one focused on location dependency with respect to mechanical characteristics [37], detecting significant regional differences. In contrast to uniaxial experiments, biaxial tests need only one quadratic tissue strip to detect anisotropic material characteristics, supporting comprehensive tissue characterisation in case less tissue is available. Further, biaxial testing is a more meaningful deformation state as it mimics the physiological loading state of UBs better than uniaxial tests. Besides an early study by Baskin et al. [6] that applied inflation tests on bovine UB tissue and a recently published work by Cheng et al. [14] realising biaxial experiments on a rat bladder wall, to the best of the authors' knowledge, only one group around M. Sacks has broadly addressed experimental characterisation in terms of biaxial testing of UB tissue [28,45,47,40,26,64,69]. The authors applied biaxial tension experiments on tissues of different animals (rat, mice, pig) to determine the mechanical characteristics in healthy and diseased (spinal cord injury) bladders. However, even after an intensive literature research, location-dependent biaxial tests on bladder tissues are not available.

For a better understanding of UB mechanics, and also as a database for three-dimensional continuum mechanical-based models, as recently proposed by Seydewitz et al. [58], microstructural information, such as fibre orientations/distributions and the proportions of the tissue constituents (elastin, collagen, SM cells) are of high interest. In particular, the combination of mechanical and microstructural data allows for the discussion of load transfer mechanisms inside the UB wall and thus enhances the understanding of UB mechanics. However, studies that focus on the mechanical characteristics as well as on the determination of all aforementioned microstructural information could be not found. In fact, only single studies that address only parts of the aforementioned issues are available [45,46,26,64,37]. Studies combining mechanical and microstructural information to enhance the functional understanding of the bladder or to create compressive input data for mechanical modelling concepts could not be found. In this regard, it is worth mentioning the recent study of Cheng et al. [14] that combined biaxial mechanical testing with multiphoton microscopy, where they were able to match the percentage of collagen fibres straightened with the stress-strain curve of rat bladder wall specimens.

Within the present investigation, we examined the location-dependent mechanical and microstructural behaviour of porcine UB. To this end, equibiaxal tension experiments were performed on three regions (apex, body, and trigone, see Fig. 1 (c)) of the UB. Within each of these regions, the tissue was tested at three different locations. To interpret the resulting mechanical responses, microstructural information was additionally determined at the identical locations. Consequently, histological analyses were conducted, and the main constituents of the UB were determined to be SM cells, extracellular matrix (ECM, including collagen and elastin), and fat as well as the location-dependent smooth muscle fibre bundle orientations.

2. Materials and methods

2.1. Urinary bladder and sample dissection

In this study, twenty-eight ($n = 28$) urinary bladders of domestic pigs (*Sus scrofa domestica*), that were 3 to 5 months old and about 90 kg in weight, were obtained from a slaughterhouse immediately after animal sacrifice and transported within 20–30 min to the laboratory. During the transport, preparation, and handling, the organs/tissues samples were directly stored in calcium-free Krebs solution ([50]: 113 mM NaCl, 4.7 mM KCl, 1.2 mM $MgSO_4$, 25 mM $NaHCO_3$, 1.2 mM KH_2PO_4, 5.9 mM dextrose, 3.3 $CaCl_2$, 1 mM EGTA) at 4 °C. The calcium-free solution was used to prevent spontaneous contractions, especially during biaxial testing, as they would distort the results.

Prior to mechanical testing, the UBs were measured and weighed in their deflated, unstretched state, cp. Fig. 1(c). The average sizes were 99.9 ± 10.1 mm in projected length (L_{long}) and 66.8 ± 6.2 mm in projected width (L_{circ}), and the mean weight was found to be 51.9 ± 9.9 g. Within the animal body, the UB is mounted on the *Ligamentum vesicae laterale* and *Ligamentum vesicae medianum* proceeds along the longitudinal axis of the bladder [8,29], see also Fig. 1(a) and (b). Along these ligaments, the bladder was sliced, dividing the bladder into three tissue parts indicated by D (dorsal) and V (ventral), cp. (d). From each part, three square samples (20×20 mm) were dissected, matching their orientation with the longitudinal and circumferential axes of the bladder and labelled as D_i and V_j, respectively. Overall, ninety ($n = 90$) samples were used during this study, one-half for mechanical (Section 2.2) and the other half for histological (Section 2.4) analyses. For the

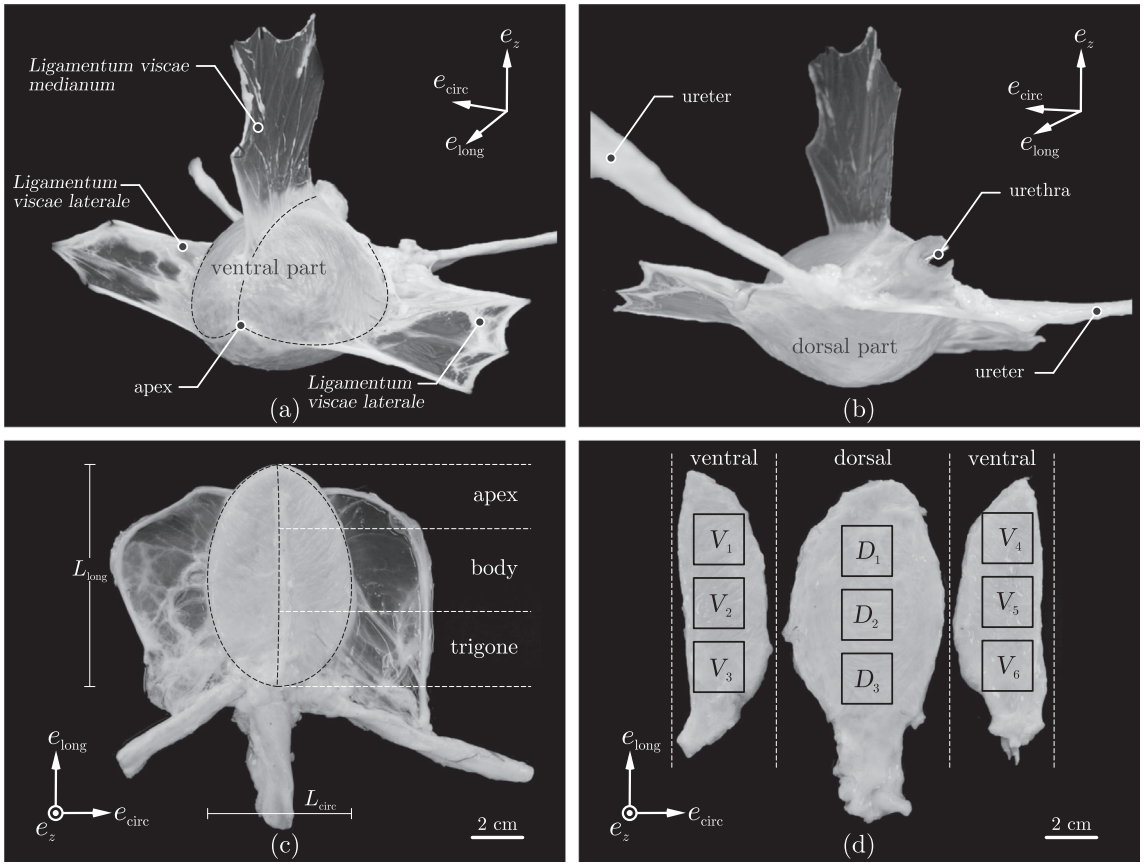

Fig. 1. Porcine bladder anatomy and tissue sample dissection. (a) Anterior and (b) posterior view of the UB with extended ligaments. While the ventral part is clearly visible in (a), the dorsal part is clearly shown in (b). (c) Top view of the deflated UB for measuring the projected dimensions (L_{long} and L_{circ}). Based on the anatomy of the UB, it can be divided into the apex, body, and trigone. For experimental investigations, the bladder was sliced into three tissue parts from which, in sum, nine samples were dissected. (d) Sample locations from the bladder's outside view. Note, black dashed lines indicate dissection paths.

statistical analyses, it was necessary to group several samples into individual regions according to the anatomy of the UB, see Table 1.

2.2. Mechanical tests

2.2.1. Biaxial testing equipment

A planar biaxial extension testing machine (Zwick GmbH & Co. KG, Germany), comprising four linear actuators that can be controlled independently, by force, position, or stretch, was used to perform the mechanical tests. The force measurement was realised by lowerable load cells, two in each direction $\boldsymbol{e}_{circ}$ and $\boldsymbol{e}_{long}$, see Fig. 2(a), which were linked to mounting devices. Each of the four mounting devices consisted of a U-shaped aluminum profile pierced by a bolt where a five-hook-cord-set was threaded. The load cells featured a maximum testing load of 50 N, with a resolution of 1 mN. Immediately above the specimen, a video extensometer with a minimum resolution of 0.4 µm (Video Extensometer ME46, Messphysik Materials Testing GmbH, Austria) was mounted to track the markers on the specimen during testing. The video extensometer was coupled with a biaxial testing machine in such a way as to control the movement of the actuators. The marker tracking was carried out by a monochrome CCD camera detecting the light-to-dark transitions on the specimen surface, generating a digital pixel image in 256 shades of grey. The data record was processed in real time by software (videoXtens, Zwick GmbH & Co. KG, Germany) following the markers during deformation. Load cell values, actuator positions, and marker displacements were recorded at 20 Hz and used for data analysis; see Section 2.3.

Table 1
Bladder regions used within the present study, cp. Fig. 1(c) and (d). Note, the regions are based on the grouping of single sample locations circumferentially and longitudinally.

region	sample locations	region	sample locations
A (apex)	V_1, D_1, V_4	*D* (dorsal)	D_i, for i = 1, …, 3
B (body)	V_2, D_2, V_5	*V* (ventral)	V_j, for j = 1, …, 6
T (trigone)	V_3, D_3, V_6		

2.2.2. Sample processing

Each dissected square sample, see Section 2.1, was fastened with 20 hooks (five per sample side) regularly distributed along the sample edges, with a 3.25 mm hook-to-hook distance and 2.0 mm corner hook distance [22], cp. Fig. 2(b). Each set of five hooks was connected via one cord. Thereby, the first and fifth hooks were tied with the cord, and the remaining three hooks were linked to the cord in such a way that they can move along the cord. This arrangement allowed the adjustment of the cord length for each hook, preventing uneven distribution of the force along the specimen side. Black circular markers (diameter 1 mm) distributed in a nine-dot square grid (3 mm distance between the markers) were glued on the upper side of the specimen to enable in-plane deformation measurement via the video extensometer, cp. Fig. 2 (b) and (c). With these dimensions at hand, the central tracking area (area bordered by the markers) was approximately 14% of the stretched area (area bordered by the hooks). Homogeneous stress/strain distribution has been observed within 16% of the center region in specimens biaxially tested using suture attachments

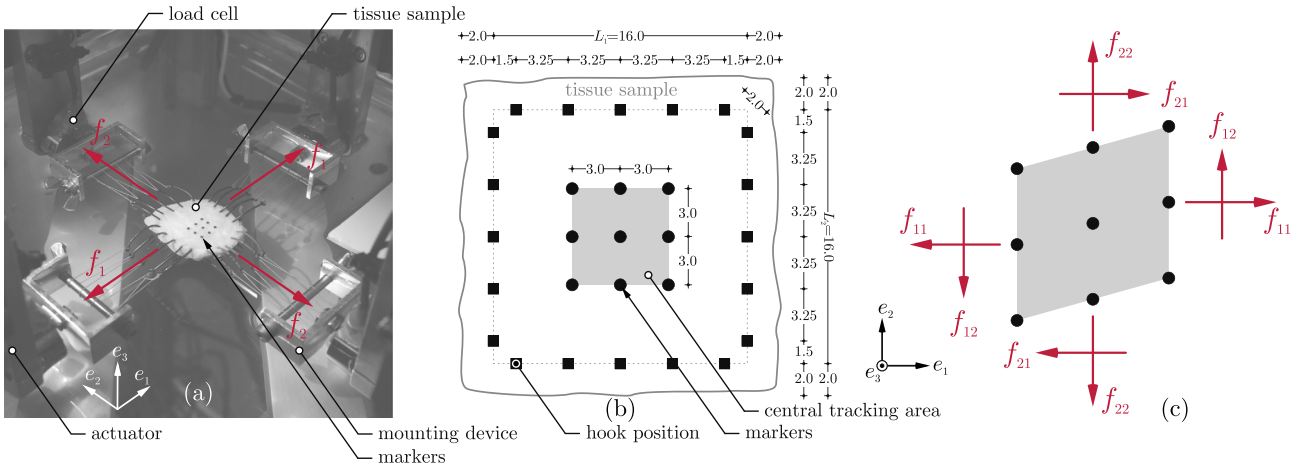

Fig. 2. Experimental setup: (a) View of the tissue specimen mounted in the testing machine. Idealised illustrations (b) of the marker (filled cycles) and hook (filled squares) positions and (c) of the forces acting on the tracked area. Note, the dimensions are given in millimetres, and the directions 1, 2, and 3 of the coordinate system correspond to the circumferential, longitudinal, and z-direction in Fig. 1, respectively.

[62]. Finally, the prepared specimen was positioned on the mounting devices of the biaxial machine and submerged in calcium-free Krebs solution at 37 °C continuously bubbled with a gas mixture of 95% O_2 and 5% CO_2. For all mechanical tests, a preload of 5 mN was applied in both axes to remove the weight effect and ensure the correct measurement of the initial markers distance in-plane.

2.2.3. Testing protocol

Location-dependent material characteristics of forty-five ($n = 45$) samples, five for each of the nine locations illustrated in Fig. 1(d), were stretch-controlled tested between 2 and 12 h after sacrifice. Thereby, the following protocol was realised: The specimens were preconditioned through 12 successive stretch-controlled cycles, ranging from 1.3 to 1.4, cp. Fig. 3(a). Note, the sub-figure displays the stretch-time relationship. The number of cycles was determined during a preliminary test, demonstrating a reproducible response of the tissue. After the last preconditioning cycle, the specimen was allowed to recover to the initial preload. Depending on the specimen, this continued for up to 30 s. After this recovery phase, we defined this state of the tissue specimen as the "stable reference state" (marked by green point), from which the final experiments were performed, see (b). In doing so, equibiaxial tensile cyclic tests at different subsequently applied stretch levels $\lambda = 1.1$, 1.2, 1.3, and 1.4, were realised, starting from the "stable reference state" marked by the green point in Fig. 3(b). For each stretch level, three cycles were performed. All tests were performed at a strain rate of $\dot{\varepsilon} = 0.2\%\,\mathrm{s}^{-1}$.

2.3. Data analysis – determination of shear deformations and stresses

By applying classical, stretch-controlled biaxial tension experiments, as realised within this study, two forces (f_1 in the circumferential and f_2 in the longitudinal direction) were measured, see Fig. 2(a). However, due to the microstructure and different constituents featuring different mechanical characteristics, the UB tissue is inhomogeneous and anisotropic, which in turn may lead to shear deformation and thus to shear forces. Consequently, all forces (two normal f_{11}, f_{22} and two shear forces f_{12}, f_{21}) acting on the tissue sample, cp. Fig. 2(c), are unknown. Information regarding the presence of normal and shear forces is essential when characterising biological tissues. However, in general, there are two strategies in the literature to determine these unknown forces. While the representatives of the first idea aim to measure the shear force directly by realising advanced experimental setups (e.g. [57,73,16]), the other group uses the two forces f_1 and f_2 and establishes additional force/stress-related equations, thus allowing

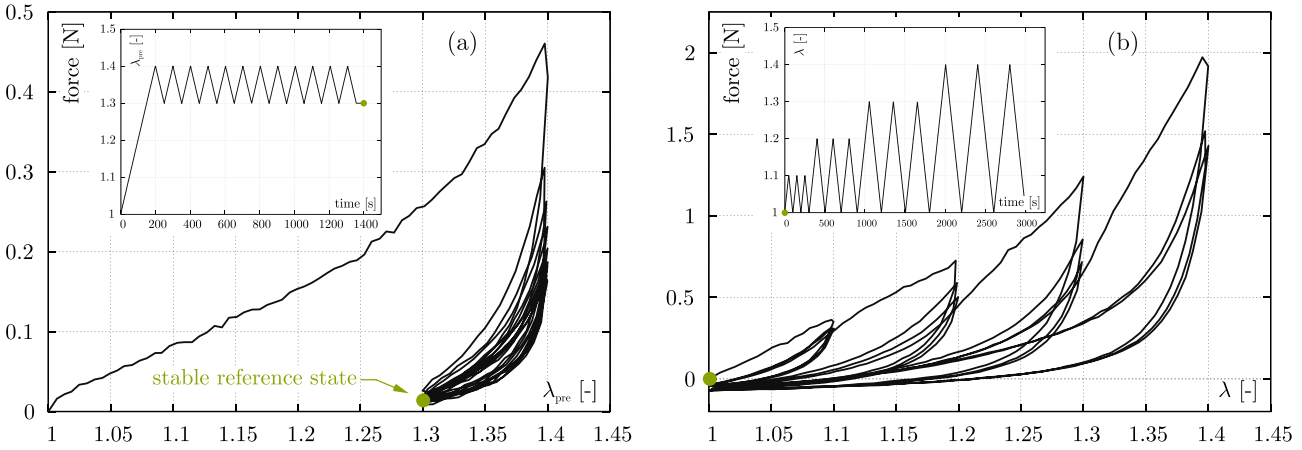

Fig. 3. Testing protocol realised within this study. (a) Equibiaxial tissue preconditioning through twelve successive stretch-controlled cycles, ranging from 1.3 to 1.4. After a phase, where the tissue was allowed to recover to its initial preload, see subfigure, three equibiaxial cyclic tests at different subsequently applied stretch levels $\lambda = 1.1$, 1.2, 1.3, and 1.4, were realised, see (b). The green points refer to the so-called "stable reference state". Note, for the sake of clarity, the testing protocol for only one loading direction is presented.

the determination of the unknown forces in a post-processing step (e.g. [32,28,60]).

Even after an intensive literature research, no quantitative statements regarding the existence or the amount of shear deformation/stresses acting on porcine UB tissue tested biaxially could be found. For a biaxial extension test of rat bladder specimens, shear effects have been assumed to be negligible [28,47,70]. Biaxial extension tests of porcine bladder samples have been performed only on delaminated sublayers of the urinary bladder wall (submucosa and lamina propria together with epithelialis), where the shear components were reported negligible without further discussion of the method employed to quantify them [26]. Thus, we followed the procedure of Sommer et al. [60] where homogeneous deformations within the central tracking area as well as tissue incompressibility is assumed to quantify the extent of shear deformation/stress. As a result, the in-plane deformations were numerically determined in a post-processing step for all sampled UB specimens. Based on the coordinate system as presented in Fig. 2 (c), we obtain

$$\lambda_1 = \frac{\partial u_1}{\partial X_1} + 1\,, \quad \lambda_2 = \frac{\partial u_2}{\partial X_2} + 1 \quad \text{and} \quad \lambda_3 = \frac{1}{\lambda_1\lambda_2 - \gamma_1\gamma_2} \tag{1}$$

with

$$\gamma_1 = \frac{\partial u_1}{\partial X_2} \quad \text{and} \quad \gamma_2 = \frac{\partial u_2}{\partial X_1}. \tag{2}$$

Herein λ_i define the stretches, u_i the displacements, X_i the reference coordinates, and γ_i denote the measures of the in-plane shear. Having further the dimensions of the undeformed specimen in form of the lengths in both directions (L_1, L_2) and the thickness (T) as well as the forces acting on the tracked areas as illustrated in Fig. 2 at hand, the normal stresses

$$\sigma_{11} = \lambda_1 \frac{f_{11}}{L_2 T} + \gamma_1 \frac{f_{21}}{L_1 T} := \sigma_{\text{circ}} \quad \text{and} \quad \sigma_{22} = \lambda_2 \frac{f_{22}}{L_1 T} + \gamma_2 \frac{f_{12}}{L_2 T} := \sigma_{\text{long}} \tag{3}$$

as well as the shear stress

$$\sigma_{12} = \lambda_2 \frac{f_{21}}{L_1 T} + \gamma_2 \frac{f_{11}}{L_2 T} = \lambda_1 \frac{f_{21}}{L_2 T} + \gamma_1 \frac{f_{22}}{L_1 T} = \sigma_{21} := \sigma_{\text{shear}} \tag{4}$$

can be straightforwardly calculated and will be used in the following section.

2.4. Histological investigations

For the histological analyses forty-five $(n = 45)$ square samples, five from each of the nine positions illustrated in Fig. 1(d), were fast frozen directly after dissection by immersing them in liquid isopentane (−160° C), which in turn was cooled down with liquid nitrogen −210 °C), consequently realising a constant vitreous form through the sample [24]. Each frozen sample was cut into two parts from which cross-sectional and in-plane slices were obtained. A cryomicrotome was used to cut five successive in-plane slices (thickness 6 μm) within the tunica muscularis, with approximately 1 mm separation between each and two cross-sectional slices.

The Picro-Sirius red staining protocol was used for collagen and smooth muscle cell differentiation. For details of the protocol, the reader is referred to the Appendix E. All histological sections were digitised using a digital microscope (ZEISS Smartzoom 5) and evaluated using the image-analysis software ImageJ (Fiji project, NIH, USA). The microstructure of the UB tissue was determined by the thicknesses of the layers, the composition of the muscular layer, and the SM fibre bundle orientation.

The thicknesses of the mucosa, submucosa, muscularis, and serosa layers were measured perpendicular to the bladder's outer surface from the digitised cross-sectional slices. The total wall thickness was then calculated by summing up all layer thicknesses. Due to slight variations in the layer thicknesses within a single cross-section, the most regular portion of the slice was measured. One measurement per cross-section was realised; thus, because there were two cross-sections per sample and five samples per position, the average of the ten measurements is reported in the following.

The composition of the muscular layer was evaluated as the amount of SM cells, ECM, and fat in the in-plane slices within the region of interest (ROI) to be 62 ± 12.7 mm^2. Two different thresholds were automatically applied to quantify each constituent by means of the percentage of pixels of each colour [67]. For the ECM, enhanced in red by the Picro-Sirius red staining, the default threshold over the green channel correctly isolated the red pixels. For the fat cells, which appear white in the stained slices, a fixed threshold of 170 (greyscale value between 0 to 255) in the blue channel isolated the white pixels. Since the software directly provides the percentage of pixels within the threshold with respect to the total of the ROI, one hundred percent minus the percentage of ECM and fat corresponds to the smooth muscle cell content. Considering that breakages of the sample appeared white (background colour) in the slices, outlier values in the amount of fat were manually checked. Additionally, an extra bladder i.e. nine samples, was fast frozen, cryosectioned, and stained with Elastica van Gieson staining to examine the characteristics of the elastin fibres within the ECM. Details of the staining protocol can be found in the Appendix F.

The muscle fibre bundle orientation was assessed directly in the digitised image based on the evaluation of the structure tensor of every pixel within the ROI. Structure tensors can be used to compute predominant directions in the local neighbourhood of a pixel and are frequently used in image processing and computer vision [9]. The algorithm was fully implemented in a macro for ImageJ and provided a histogram of the orientation from −90° to 90° weighted by the coherency and the energy values calculated from the structure tensor [53]. The predominant orientation corresponding to a specific location and level was calculated by the mean and standard deviation of the peak value of the orientation histograms $(n = 5)$ weighted by the amount of the peak, i.e. highly oriented samples have more weight than those that are scattered. The same ROI was used for composition and orientation analyses, as ROI was initially aligned with the circumferential and longitudinal axes of the bladder.

2.5. Statistical analysis

Statistical analyses were conducted to discover whether the stress-stretch response of every location and region was significantly different with respect to the others and to determine if the UB wall had an anisotropic mechanical response. The statistical analyses were accomplished as follows. First, a Shapiro-Wilk test was used to check the data for normal or non-normal distribution. Second, a two-tailed t-test was used for normally distributed data sets and a Wilcoxon-Matt-Whitney test for non-normally distributed data sets. For the analysis of anisotropy, where the response in the circumferential axis was compared to the longitudinal axis of the same specimen, a paired analysis was chosen. Significant differences were defined as $p < 0.05$. All statistical

analyses were performed using R statistical software (R-project, Austria).

3. Results

3.1. Urinary bladder mechanical properties

Typical preconditioning and measuring cycles during equibiaxial loading in terms of Cauchy stress vs. stretch are depicted in Fig. 4 to be consistent in all test specimens. During the first four to six preconditioning cycles (a), a change in the maximum stress was clearly visible. Between cycles 8 to 12, the curves were stable and showed a repeatable behaviour (differences in peak values $< 2.5\%$ between the cycles). After a recovery phase, where the tissue was allowed to return to its initial preload, the specimen was loaded by three cycles at different subsequently applied stretch levels $\lambda = 1.1$, 1.2, 1.3, and 1.4, see Fig. 4(b). The first two cycles were sufficient to achieve a stable and repeatable behaviour. Consequently, between the second and third cycle, the change in the maximum stress value was very small. Softening was observed between subsequent stretch levels occurring mainly in the first cycle of each increased stretch level, as evident in Fig. 4(b). Between the first and the two last cycles, a clear decrease in the hysteresis area was observed, see Fig. 4(b). The last cycle was used as a representative measuring cycle and was used in the following illustrations. The aforementioned material characteristics can be found more or less for both loading directions.

Following Fig. 5, mean values (lines) and standard deviations (shaded areas) of five single tests are presented in terms of Cauchy stress vs. stretch for nine different locations, cp. Fig. 1(d). Independent of the specimen's excision location, the tissue strips showed similar qualitative properties, characterised by an exponential, non-linear behaviour combined with notable hysteresis areas during loading/unloading. Longitudinal and circumferential stress-stretch curves presented the same curve progression, although the stresses in the longitudinal direction (dashed lines) appeared to be slightly higher than in the circumferential direction (solid lines).

In order to identify regional differences within the UBs, the sample locations were grouped into circumferential (A, B, T) and longitudinal (D, V) regions, cp. Table 1 and Fig. 1(d). In Fig. 6, the stress-stretch curves for apex (a), body (b), and trigone (c) regions are presented for comparison reasons. The mean peak stresses in the trigone region were more than 40% higher compared to the apex and the body regions; however, due to biological variation, statistical significance was only reached at the very peak. On the other hand, Fig. 7 compares the mechanical response of the ventral (a) and dorsal (b) regions, where both regions yielded similar peak stress values.

In Table 2, the p-values from the statistical analysis of anisotropy reported in terms of circumferential stress versus longitudinal stress (of the same sample) for all sample locations and regions are presented. Of the nine sample locations, only V_5 revealed a significant pattern of anisotropy. By grouping the samples circumferentially, the apex, body, and trigone regions also failed to showed significant anisotropic behaviour. However, by sorting them longitudinally into two groups, dorsal and ventral, the ventral region exhibited a significant anisotropic response ($p = 0.003$), while the dorsal region did not show significant differences between directions ($p = 0.978$); see also Fig. 7. To quantify the response, the degree of anisotropy was measured in terms of circumferential stress divided by longitudinal stress for each test. Thus, for isotropic material characteristics $\sigma_{\text{circ}}/\sigma_{\text{long}} = 1$, the ventral side of the porcine UB presented a degree of anisotropy of $\sigma_{\text{circ}}/\sigma_{\text{long}} = 0.85 \pm 0.28$, whereas the dorsal side was completely isotropic $\sigma_{\text{circ}}/\sigma_{\text{long}} = 0.99 \pm 0.35$.

The area enclosed by the loading and unloading curves, known as hysteresis, reflects the dissipated energy per unit volume. The absolute energy dissipated (E_{abs}) was computed as the difference between the loading and unloading area underneath the stress-stretch curves, while the relative energy dissipated (E_{rel}) was calculated as a percentage with respect to the loading curve. Table 3 summarises the hysteresis values in the circumferential and longitudinal directions at each stretch level for the average response of all samples tested. Both directions presented similar hysteresis behaviours, i.e. approximately one-half of the energy was dissipated at all stretch levels. From cycle to cycle, a wide difference in the hysteresis area between the first and the subsequent cycles was observed, see also Fig. 4(b). During the first cycle, the hysteresis area was larger than 70%, while the hysteresis areas were closer to 50% during the second and third cycles. Comparing the hysteresis areas among the regions, see Table 9 in Appendix B, it is noteworthy that E_{abs} in the dorsal region D was the same in both directions, while in the ventral region V, the absolute energy dissipated in the circumferential direction was approximately 0.8 of that in the longitudinal direction.

The shear patterns assessed from the nine-dot-grid deformation gradient presented a large variance across samples. To provide a descriptive overview of the shear behaviour, the mean of the absolute values was computed and is summarised in Table 4.

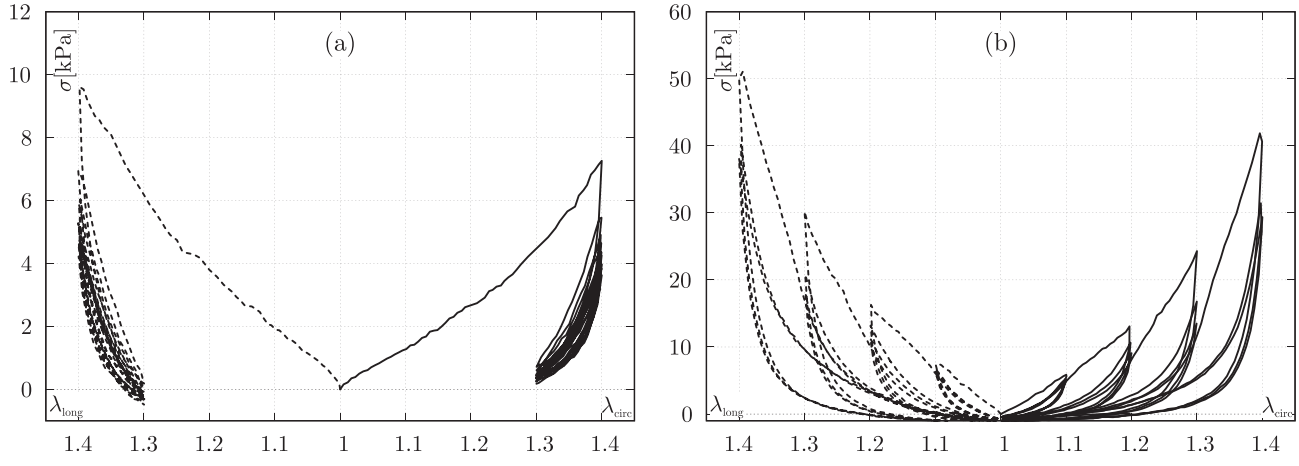

Fig. 4. Representative mechanical response in the longitudinal (dashed lines) and circumferential (solid lines) directions in terms of the Cauchy stress vs. the stretch with respect to the testing protocol, provided in Fig. 3: (a) Tissue preconditioning through twelve successive stretch-controlled cycles, ranging from 1.3 to 1.4. (b) Measuring cycles at different subsequently applied stretch levels $\lambda = 1.1$, 1.2, 1.3, and 1.4.

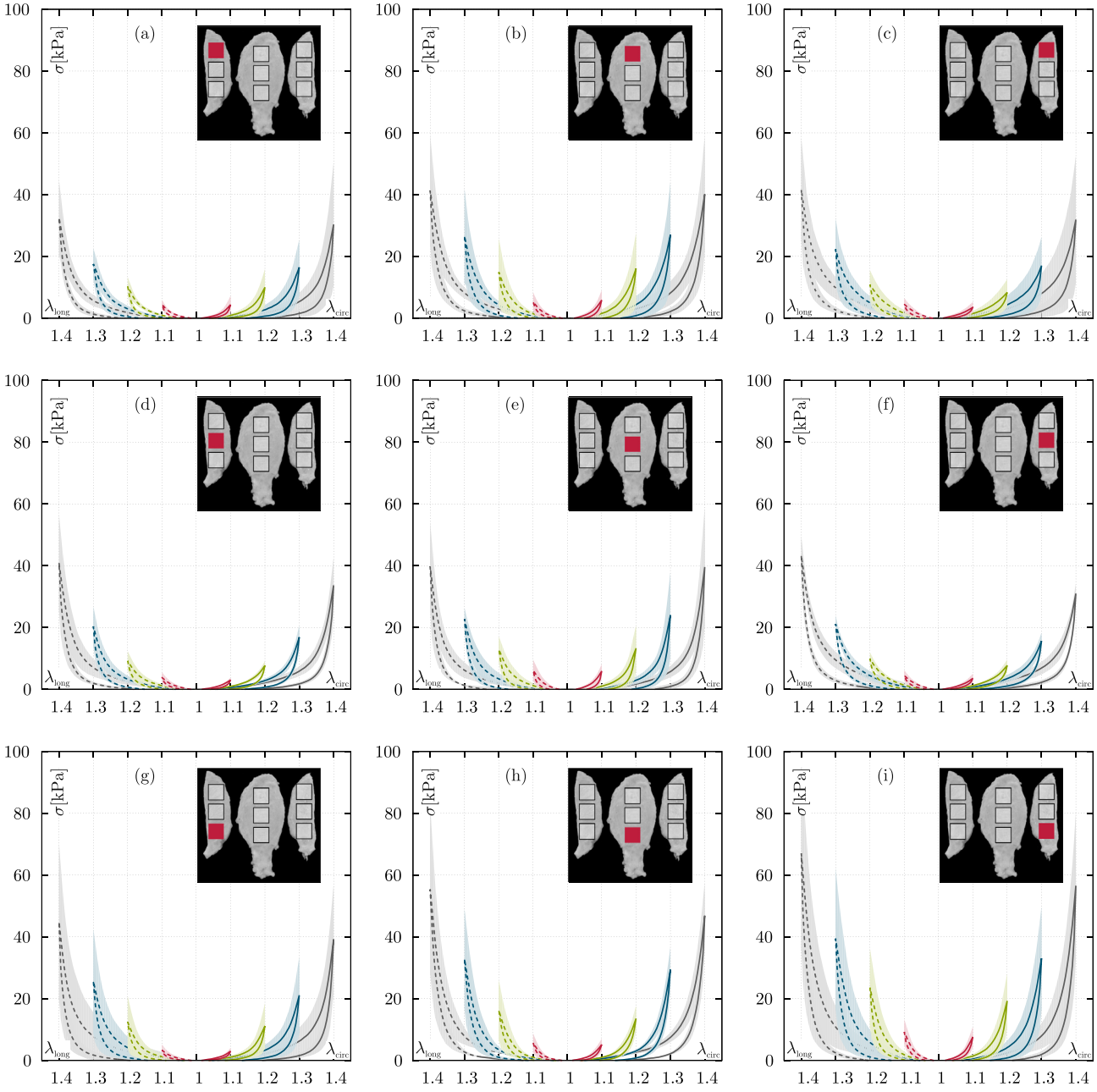

Fig. 5. Location-dependent stress-stretch behaviour of the UB wall. Lines (solid and dashed lines indicate the stress-stretch responses in the circumferential and longitudinal directions, respectively) characterise mean values, and the shaded areas depict the standard deviations, each calculated from five single tests.

For detailed region-specific values, the reader is referred to Table 10 in Appendix B. In general terms, the shear deformation was determined to be larger in the longitudinal direction than in the circumferential direction. The ratios of shear to normal stress increased with increasing stretch from 1 to 2.5%. In other words, on average, the shear stress was between 40 and 100 times smaller than the normal stress and thus negligible. No particular differences in shear were observed among the different regions.

3.2. Urinary bladder microstructure

The thicknesses of the different layers within the UB wall for each sample location and region are provided in Table 5. The main difference among the regions was found in the trigone region *T*. Meanwhile, the serosa, submucosa, and mucosa layers presented uniform thicknesses for all locations, 0.14, 0.43, and 0.76 mm, respectively; the tunica muscularis became thinner in region *T*, 3.95 mm compared to 4.87 and 5.01 mm in regions *A* and *B*, respectively. No thickness differences were observed between the dorsal and ventral regions.

The numbers of SM cells, ECM, and fat in the tunica muscularis are summarised in Table 6. For detailed region-specific composition, see Appendix C. No particular differences were found between various regions. In short, the detrusor was composed of 63.7% SM cells, 32.6% ECM, and 3.7% fat. The thickness of the muscle bundles varied between 400 and 800 μm, and the diameter of the fat cells was approximately 50 μm. SM cells and ECM content appeared constant throughout the detrusor thickness. However, the amount of fat varied between the slices. The higher percentages of fat were measured in the middle sections (ip2 and

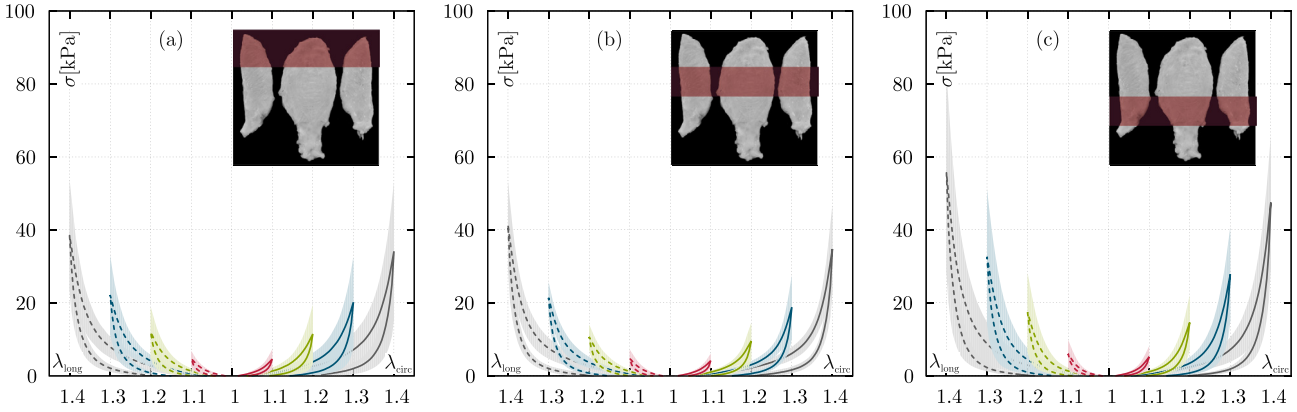

Fig. 6. Average stress-stretch behaviour of the three UB physiological regions: (a) apex, (b) body, and (c) trigone. Lines (solid and dashed lines indicate the stress-stretch responses in the circumferential and longitudinal directions, respectively) characterise mean values, and the shaded areas depict standard deviations. For maximum and minimum stress values, the interested reader is referred to Table 7 in Appendix A.

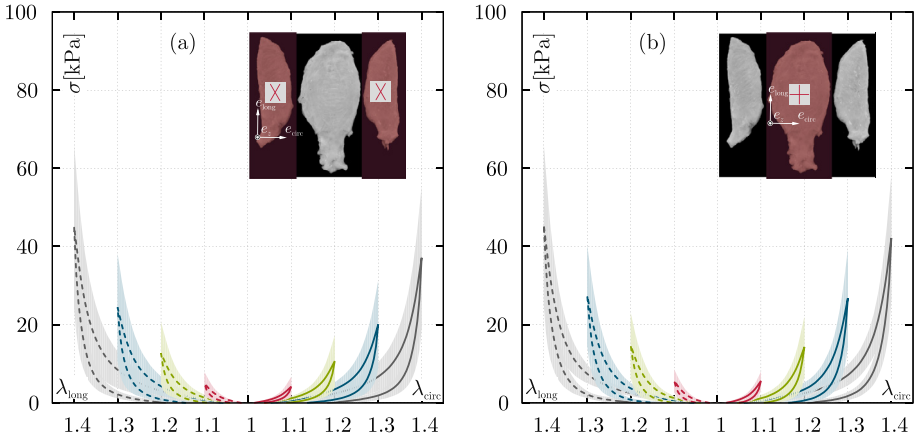

Fig. 7. Comparison of the mechanical behaviour and the fibre bundle orientation of the ventral (a) and dorsal (b) regions. The ventral samples presented a 60°/120° cross-fibre orientation through the wall, yielding an anisotropic mechanical response, while the dorsal samples presented with a perpendicular cross-fibre orientation show an isotropic response. Solid and dashed lines indicate the stress-stretch responses in the circumferential and longitudinal directions, respectively. See Fig. 8 for more details of the fibre orientation. For maximum and minimum stress values, the interested reader is referred to Table 8 in Appendix A.

Table 2
Level of significance expressed by p-values of the anisotropy (comparison of the response in the circumferential and longitudinal directions of the same sample) for all sample locations and regions. Note, the p-value reported was the highest calculated of the four stretch levels ($\lambda = 1.1, 1.2, 1.3, 1.4$) for each sample location and region. Note, * indicates significant anisotropy.

single sample locations									sample regions, grouped according to Table 1				
V_1	D_1	V_4	V_2	D_2	V_5	V_3	D_3	V_6	A	B	T	V	D
0.934	0.999	0.310	0.374	0.999	0.015*	0.506	0.813	0.167	0.639	0.169	0.095	0.003*	0.978

Table 3
Hysteresis areas in terms of dissipation energy per unit volume of the average stress-stretch curve of all samples ($n = 45$) obtained during equibiaxial testing at four stretch levels. The absolute energy dissipated (E_{abs}) and the relative energy dissipated (E_{rel}) regarding the areas under the loading curves (here the conjugated quantities 1st Piola-Kirchoff stress and stretch are used) in the circumferential and longitudinal directions are given. For a region-specific presentation of the hysteresis, the reader is referred to Table 9 in Appendix B.

stretch ratios	hysteresis area			
	circumferential		longitudinal	
λ	E_{abs}	E_{rel}	E_{abs}	E_{rel}
–	[J/m^3]	[%]	[J/m^3]	[%]
1.1	52	48	56	47
1.2	202	52	223	52
1.3	459	54	524	54
1.4	887	55	1002	55

Table 4
Average shear behaviour of all samples tested ($n = 45$). The values were computed as the means of the absolute values at each stretch level. For region-specific values, see in Table 10 in Appendix B.

stretch ratios	shear deformation		shear stress	stress ratios	
λ [–]	γ_{circ} [–]	γ_{long} [–]	σ_{shear} [kPa]	$\sigma_{shear}/\sigma_{circ}$ [%]	$\sigma_{shear}/\sigma_{long}$ [%]
1.1	0.022	0.022	0.050	1.2	1.0
1.2	0.034	0.037	0.183	1.7	1.5
1.3	0.043	0.048	0.398	2.1	1.7
1.4	0.052	0.062	0.893	2.5	2.1

Table 5
Location- and region-specific layer thicknesses of the UB wall in millimetres, cp. Fig. 8(a).

	single sample locations									sample regions, grouped according to Table 1				
Layer	V_1	D_1	V_4	V_2	D_2	V_5	V_3	D_3	V_6	*A*	*B*	*T*	*V*	*D*
serosa	0.16	0.16	0.12	0.12	0.15	0.12	0.13	0.15	0.12	0.15	0.13	0.13	0.13	0.15
muscularis	4.66	4.83	5.13	4.94	5.26	4.83	4.01	4.06	3.78	4.87	5.01	3.95	4.56	4.72
submucosa	0.44	0.32	0.43	0.52	0.40	0.41	0.45	0.46	0.45	0.40	0.44	0.45	0.45	0.39
mucosa	0.84	0.70	0.78	0.88	0.85	0.76	0.60	0.73	0.68	0.77	0.83	0.67	0.76	0.76
total	**6.10**	**6.01**	**6.46**	**6.46**	**6.66**	**6.12**	**5.19**	**5.40**	**5.03**	**6.19**	**6.41**	**5.21**	**5.89**	**6.02**

Table 6
Number of the various constituents in the tunica muscularis, determined from the outermost section (ip1) adjacent to the serosa layer to the innermost section (ip5) next to the submucosa layer, cp. Fig. 8. The distance between the in-plane slices was 1 mm in the *z*-direction. For region-specific values, the interested reader is referred to Fig. 11 in Appendix C.

in-plane slice	SM [%]	ECM [%]	fat [%]
ip1	63.4	33.0	3.6
ip2	64.5	31.0	4.5
ip3	63.7	31.9	4.4
ip4	63.0	33.5	3.6
ip5	63.8	33.7	2.5
mean ± s.d	**63.7 ± 2.1**	**33.6 ± 1.9**	**3.7 ± 1.3**

ip3), while they were lowest in the deepest section (ip5) adjacent to the submucosa.

Elastin fibres were observed scattered throughout the ECM, running tangled within the collagen network following approximately the orientation of the closest muscle bundle. These fibres of diameter 0.8 μm and lengths varying between 40 and 80 μm constituted less than 2% of the ECM content, i.e. <0.6% of the total.

Fig. 8 shows the orientation of the muscle fibre bundles throughout the tunica muscularis (stack of five slices) for each sample location. Different orientations in the outer (slices ip1 and ip2) and inner parts (slices ip4 and ip5) of the tunica muscularis were observed in all positions. Therefore, these two muscle bundle arrangements can be counted as two sublayers of similar thickness. The in-plane slice ip3 fell between both arrangements, leading the orientation in these slices to present high dispersion with no predominant direction. This was true for every sample location except for D_1, where ip3 still belonged to the outer sublayer, and ip4 was the slice caught between both arrangements, i.e. high dispersion and non-representative orientation. The fibre orientation of the outer sublayer was cross-oriented with respect to that of the inner, between 60° and 90°, depending on the sample location, cp. Fig. 1(d). Specifically, the samples on the dorsal region *D* of the bladder were highly oriented circumferentially in the outer part of the tunica muscularis and longitudinally in the inner part. In the ventral region *V*, these sublayers were cross-oriented 60°/120°. Note that there was no continuity in the fibre orientation from one side of the *Ligamentum vesicae medianum* to the other.

Remark 1 (*Methodology implications on result interpretations*). In view of the SM fibre bundle orientation results, it is worth mentioning several practical issues. Ideally, in order to capture the spatial fibre orientation throughout the bladder, it would be to take in-plane sections proportionally distributed within the thickness of the tunica muscularis, but this was not feasible to measure *in situ*. Therefore, the approximated 1 mm separation between the slices was taken as a reference. This distance was adjusted as a function of how much sample was left in order to keep all slices in the best possibly uniformly distributed within the tunica muscularis thickness. This approximation together with the natural variability of the tissue leads to the fact that the middle slices (ip2, ip3, ip4) present larger dispersions than the first and the last in-plane sections (ip1, ip5). Especially, ip3 in some cases fell in the outer sublayer such as in locations D_1 and D_3, in other cases fell in the inner sublayer such as in locations V_2 and V_5 and in other cases just in between. Note, the mean and the standard deviation were calculated out of 5 samples. Considering that *a priori* there was no information about the spatial distribution of the SM fibre bundles in the UB wall a two-layers-arrangement can be appreciated.

It seems that the fibre bundles in the neck of the bladder come from the urethra structure, circumferentially oriented in an external layer and longitudinally oriented in an internal layer [20,74]. From here the fibre bundles run circumferentially in the external layer on the dorsal side and gradually change the orientation to the ventral side. Similarly, in the internal sublayer, which starts longitudinally in the bladder's neck, the fibre bundles run straight on the dorsal side and progressively change the orientation to the ventral side, becoming in the ventral side an oblique-cross-orientation. From dorsal to ventral the cross-orientation gradually vary from perpendicular to oblique as a function of the sample location coordinates in $\boldsymbol{e}_{circ}$ and $\boldsymbol{e}_{long}$. That is the reason why D_1, D_2, D_3, V_2, and V_5 present smaller standard deviation, in general terms, compared to V_1, V_3, V_4, and V_6 since the former were easier to reference to the bladder anatomical landmarks and the sample location had less impact than in the latter.

3.3. Relationship between mechanical properties and microstructure of the UB wall

Comparing the regional differences between the mechanical properties and the microstructure, two matches were found. First,

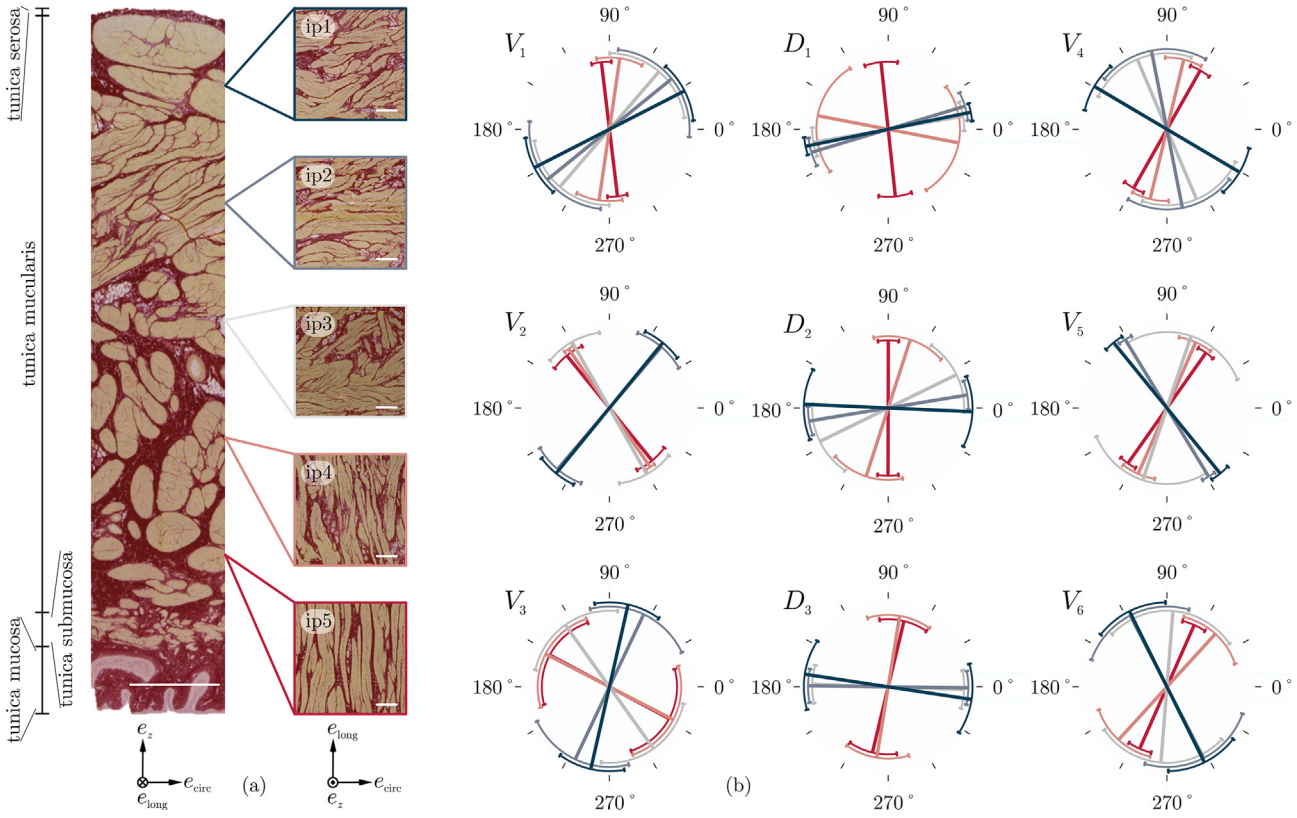

Fig. 8. Muscle fibre bundle orientation in the tunica muscularis of a UB in the *z*-direction from the outermost (ip1) to the innermost (ip5). (a) Cross-sectional and in-plane slices of the UB wall, sample location D_2. Scale bar, 1 mm. (b) Polar diagrams of muscle fibre bundle orientation for each sample location, mean orientation (radial), and standard deviation (arc). Note: Bluish in-plane slices, ip1 and ip2, correspond to the outer fibre bundle arrangement, while reddish in-plane slices, ip4 and ip5, correspond to the inner fibre bundle arrangement. ip3 falls between both arrangements, presenting high dispersion.

the mechanical properties of the circumferential regions *A*, *B*, and *T* revealed that the trigone region had more than 40% higher peak stress values. Meanwhile, the apex and body regions presented very similar stresses, cp. Fig. 6. Comparing the microstructure of these regions, the trigone region showed a thinner tunica muscularis with respect to the rest of the bladder, see Table 5. Second, from the mechanical properties of the longitudinal regions *V* and *D*, it was observed that the ventral region presented higher stresses in the longitudinal direction than those in the circumferential direction, while the response was isotropic in the dorsal region, cp. Fig. 7. This behaviour matched the muscle fibre bundle orientation within the tunica muscularis, where the outer and the inner sublayers in the ventral region were cross-oriented 60°/120°. Meanwhile, in the dorsal region, they were perpendicularly arranged; see also Fig. 8(b). For more quantitative details on the relationship between the region-specific mechanical response and its microstructure the interested reader is referred to Appendix D.

4. Discussion

The present study demonstrates that the microstructure of the UB wall is heterogeneous across the organ, and this has an impact on its mechanical properties. To the best of the authors' knowledge, this is the first study to examine (i) the mechanical properties of the UB wall through biaxial testing considering sample location; (ii) the microstructure of the UB wall in terms of layer thicknesses, composition, and muscle fibre bundle orientation; and (iii) the explicit match of mechanical and structural variation across the bladder.

4.1. Urinary bladder mechanical properties

Tissue preconditioning was conducted in order to reach an "equilibrium state", where the curves are repeatable and stable to determine the mechanical properties of the tissues. Although this step is widely used in soft biological tissue testing, there is no standardised protocol for specimen preconditioning, with the exception of some general recommendations, such as that the maximum stretch level and strain rate should match the intended test [15]. It is common to find references to the stable state in terms such as "nearly similar" or "a few percent different" [25,61,4], but it is not clear how much this deviation is. For bladder specimens, porcine, and murine samples, it is common to perform a large number of preconditioning cycles, and between ten and twelve cycles have been reported [45,26,37,70,13]. In the present study, twelve cycles were performed to precondition the UB wall specimens in reaching a sufficient stable stress-strain relationship with a steady loss of 2.5% per cycle over the last four cycles.

During preliminary studies, different preconditioning protocols were tested. The unloading curve did not return to the initial state at any stretch level. Therefore, the preconditioning cycles were limited to the range of positive forces, i.e. sample extended, allowing the specimens to recover to the initial preload state afterward. Then, the stable reference state for testing was defined. This procedure of defining the reference state after preconditioning is in accordance with the biaxial testing protocols of [70,14]. After the preconditioning protocol, specimens returned to zero stress during every cycle.

There is no consensus in the stretch range of the UB wall either. UB wall specimens have been biaxially tested up to $\lambda = 1.7$ [14] following different criteria such as force limit, stress limit, or fibre

stretch [46,47,69,13,14]. Specimens uniaxially tested have been stretched up to $\lambda = 2$ for cycling loading [72,48,31] or up to rupture in monotonic tests [37,41,58]. Note that each study has tested different samples i.e., different species, ages, layers, illnesses, or even samples chemically treated, which makes the comparison unsound. Furthermore, the preconditioning protocol has a high impact on the stretch values reported. For example, in the present study, the reference state already implies a stretch of approximately $\lambda \approx 1.3$, which means that specimens were test up to $\lambda \approx 1.7$ respect to the intact bladder. The problem is that stretches previous to the reference state is generally not measured/reported which make impossible to track back the results to the intact bladder specimen. This issue has been already pointed out by Wognum et al. [70]. They proved that for highly extensible soft tissues such as UB wall there are significant differences in the values calculated with respect to the tare-load or to the unloaded state.

The physiological stretch range of the UB wall has been not actually measured, although some values can be inferred from different observations. Korossis et al. [37] uniaxially stretched pig UB wall strips up to rupture and they suggested the physiological stretch level as the transition point in the stress-strain curves. This transition point falls between $\lambda \approx 1.8$ and 3 as function of the sample location and orientation. Parekh et al. [50] measured the surface strains of rat bladders during controlled filling. The bladders were filled up to physiological maximum volume measuring peak circumferential and longitudinal stretches of ~ 1.9 and ~ 2.3 respectively. More recently, the studies of [31,14] observed the unfolding and rearranging of the collagen fibrils under multiphotone microscopy during tensile tests of murine bladder samples. In the first study, the specimens were uniaxially tested up to $\lambda = 2$ not showing any evidence of failure at micro and macro levels and presenting completely straighten collagen fibrils between $\lambda = 1.6$ and $\lambda = 2$. In the second study, the specimens were biaxially stretched up to where the collagen fibres were visibly straightened. They reported maximum stretches between $\lambda = 1.4$ and 1.7 for adults rats and $\lambda = 1.3$ and 1.6 for aged rats.

Anisotropy was found to be a region-dependent property of the UB. This is due to the muscle fibre bundle orientation within the inner and outer parts of the tunica muscularis. Considering that both sublayers have a similar thickness, in the case of the dorsal samples, where the fibre arrangement was aligned with the axes of the testing machine (perpendicular with respect to the other), an isotropic response was captured. However, in the ventral samples, where the fibre cross-orientation was found to be approximately 60°, the projection of the fibre orientation to the biaxial testing axes (longitudinal and circumferential) was larger along the longitudinal axis than along the circumferential, which was observed in the mechanical test, where higher stresses were reached in the longitudinal direction than in the circumferential.

Presently, to the best of the authors' knowledge, there are no biaxial extension data of porcine or human UB walls. Previous biaxial studies in rat specimens defined the bladder mechanical response as isotropic under equibiaxial loads [28,14]. Because of rat UB size, the specimens tested constituted almost the whole bladder and therefore could not account for regional differences. Regarding porcine bladders, only one study dealt with regional differences across the organ [37]. Based on extra-physiological rates, they concluded that while the bladder expands uniformly circumferentially, the bladder is more compliant in the apex region longitudinally. This is somewhat comparable to our findings, where the dorsal and ventral regions showed similar stress levels, but the apex and body regions showed lower peak stress than that of the trigone region.

The UB wall exhibited pronounced viscoelastic behaviour, with hysteresis formation of 50% in both directions, indicating considerable energy dissipation during quasi-static cyclic loading. This loss of energy observed in soft biological tissues has been explained as a result of frictional processes, such as tissue fluid movement [61]. The hysteresis loop during the first cycle was much greater than that during the remaining cycles. Second and third hysteresis loops almost entirely overlapped, indicating a viscoelastic steady state, i.e. no further loss of energy [39]. Similar hysteresis behaviour has been reported for other muscular organs, such as the oesophagus and myocardium [59,61].

It was a common practice in planar soft tissue characterisation to assume negligible shear stress, as this amount was assumed to be very small compared with the principal stresses [45,59]. However, due to the challenge of quantifying shear stress during biaxial testing, the error of this assumption was unknown. Recent biaxial tests accounting for shear stress have reported it to be between 1 and 2 orders of magnitude lower than principal stresses for sclera [17] and myocardium [60].

The shear stress was estimated through the assumption of planar homogeneous deformation within the tracking area, cp. Fig. 2 (b). Note, the use of discrete strain-measurements (markers) is a limitation compared to full-strain measurements such as digital image correlation techniques. However, the use of markers was necessary to perform stretch-control tests. Digital image correlation techniques in comparison would be useful to check the homogeneity of the strain field in a post-processing step. Therefore, the used method is not an exact measurement, but it provides some hints of the impact of considering or neglecting the shear stress on the constitutive formulation of the UB wall. The ratio of normal to shear stress was quantified to be greater than 40 times for stretches up to 1.4. To the best of the authors' knowledge, this is the first time that shear stress has been estimated for bladder tissue. Gloeckner [27] mentioned that the shear deformations of rat bladder samples for stretches up to 1.12 were less than 3° during the entire testing time. According to our records, only 3 out of 45 tests exceeded 3° at $\lambda = 1.1$.

4.2. Urinary bladder microstructure

Microstructural investigations realised within the present study revealed the existence of four main layers: the tunica mucosa, tunica submucosa, tunica muscularis, and tunica serosa. The thicknesses of the serosa, submucosa, and mucosa layers appeared constant in all regions, unlike the tunica muscularis, which became thinner in the trigone region close to the urethra. The trigone is a special muscular region of the bladder that controls the micturition process together with the urethra [33,56]. According to our results, the trigone region presents a special function within the bladder, and its mechanical properties and microstructure differ from the rest of the organ.

The human UB wall is frequently divided into two parts, the lamina propria and the detrusor, because they exhibit different mechanical properties and nervous control [12,1] and because their thickness can be measured with non-invasive tests, such as ultrasound [52]. Given this division, the lamina propia would consist of the tunica mucosa and tunica submucosa, and the detrusor would include the tunica muscularis and tunica serosa. Measurements of thicknesses in human bladders have been reported to be 1.3 mm for the lamina propria and 4.4 mm for the detrusor [21], which are very similar to the porcine values measured in the present study. That is, human and porcine bladders show similar cross-sectional structure.

The composition of the muscular layer appeared homogenous across the organ, featuring a ratio of muscle bundles and collagen similar to rat bladders [51,46,30]. However, a variation in the fat content was observed in the transmural direction. A higher quantity of fat between the two muscle bundle arrangements was measured, whereas the fat content was low next to the submucosa. In the cross-section slices, small clusters of fat cells were accumulated at medium-high in the tunica muscularis, which explains the higher percentage of fat in the middle sections. Conversely, a significant decrease in fat content in the last section was highly probable due to the fact that the last section ip5 was performed very close to the submucosa layer.

No specific measurements of elastin characteristics in the ECM of the porcine UB have been found in the literature. Korossis et al. [37] observed sparse elastin fibres throughout the porcine UB wall, predominantly oriented in the circumferential direction. Similar descriptions of elastin content have been reported for human and rat bladders [44,45,30]. Murakumo et al. [44] measured diameters between 0.5 and 3.0 μm for elastin fibres on the surface of the muscle fascicles and 0.1 μm for those that are intrafascicular.

Muscle fibre bundle orientation in the UB wall has been an interesting topic of discussion in the bladder mechanics literature based on mechanical experimental results, but few data have been reported to date. Preferential longitudinal or circumferential direction has been reported equally [28,37,72,48,58]. The present study shows that the tunica muscularis is structured in two muscle bundle arrangements or sublayers of similar thickness, which change in orientation across the organ. Furthermore, this gradual change in the orientation produces different cross-orientations between sublayers, ranging between 90° in the dorsal region to 60° in the ventral region. This variation in the fibre orientation is reflected in the mechanical properties of the bladder, showing more or less anisotropy as a function of the fibre arrangement. Therefore, different sample locations may explain the inconsistency of the results reported, including the predominant orientation of the UB wall.

The present study complements the description of the collagen arrangement in the ECM of the tunica muscularis described recently for rat UB walls [30]. SM cell nuclei and collagen fibres were found to be highly aligned with the orientation of the muscle fibre bundles. Collagen appeared highly locally oriented as follows: gradual change in the orientation across the width of the UB wall, i.e. progressive in-plane orientation change, and abrupt transitions through the depth of the wall, i.e. acute transmural orientation change. Specifically, two families of collagen fibres were described at different depths of the UB wall, the outer oriented circumferentially and the inner longitudinally [31].

The arrangement of the SM layers within the tunica muscularis determined in this study fits well with the description of the bladder and urethra musculature by Woodburne [71]. The author described the urethral wall made up of an external circular layer and an internal longitudinal layer, which appeared attached continuously to the trigone. This arrangement (external circumferentially and internal longitudinally) was observed in our results, as well. The latest studies describe a similar single continuous smooth muscle structure of the bladder and the urethra [33,20,74].

4.3. Functional aspects on relation to mechanical findings

From the physiological point of view, the UB lies within the peritoneal cavity and is attached to the abdominal wall via three ligaments oriented longitudinally on the UB surface, see Fig. 1. The ventral *Ligamentum vesicae medianum* connects the bladder to the linea alba and pelvic symphysis, and the two *Ligamenta vesicae laterale* attach it to the pelvic walls. We found slightly higher stiffness longitudinally compared to circumferentially, which can be attributed to a more longitudinal arrangement of muscle fibre bundles; see Fig. 8(b). Consequently, bladder deformation during filling might be more pronounced in the circumferential direction than in the longitudinal direction, reducing the strain of the three longitudinally orientated ligaments on the UB surface. Moreover, the UB is connected by the urethra to the urethral orifice, which is situated above (dorsal and caudal) the UB (in the standing pig). During bladder filling, gravitational force (of urine) might result in longitudinal tensile forces in the bladder wall, which can be compensated by a more longitudinal orientation of muscle fibre bundles. The observed higher stiffness of the trigone, cp. Fig. 6 (c), which is nearest to the urether, might be a further adaptation of the UB to withstand these loading situations. As the trigone is a region with enhanced sensitivity [35], another possible reason for higher stiffness of the trigone compared to the body and apex might be the protection of nerve tissue against large deformations induced by bladder filling.

4.4. Impact on bladder modelling

From the computation point of view, the UB wall has a complex mechanical behaviour with passive and active responses of its multi-layered structure. Initial approaches came from the modelling of smooth muscle contraction seeking the mathematical description of the mechano-electrochemical process triggering the muscle contraction [10,36,3]. These models are characterised by the formulation of the interaction between the different fields at cell level regardless of the organ geometry. Another approach proposed a fibre-reinforced visco-hyperelastic constitutive model for the passive behaviour of the UB wall based on uniaxial tests [48]. The latest UB model includes both approaches, active and passive behaviours of the different layers, describing the mechano-electrochemical smooth muscle contraction process together with the non-linear passive response. The formulation, based on active and passive experimental data, it is implemented in a three-dimensional realistic geometry [58]. This model, although it is an important step forward in the simulation of the bladder behaviour at organ level, do not address the heterogeneous mechanical and structural properties of the bladder. The region-specific data release in the present study will help in the refinement of such approaches.

5. Conclusion

The porcine UB presents morphological and mechanical heterogeneity across the organ. Two muscle fibre bundle arrangements were found within the muscularis layer, each of them cross-oriented with respect to the other, featuring a varying relative angle between them to be a function of the location in the bladder. It was also observed that the tunica muscularis was thinner in the trigone region, close to the urethra. Regarding the mechanical properties, the UB wall showed a non-linear viscoelastic behaviour under equibiaxial loading, being isotropic in the dorsal region and anisotropic in the ventral. Furthermore, the trigone reached higher stress levels at the same stretch as that of the apex and body regions.

Acknowledgements

Partial support for this research was provided by the Deutsche Forschungsgemeinschaft (DFG) under Grants BO 3091/9-1 and SI 841/9-1. Furthermore, the authors would like to thank Marco Iovaldi for implementing the quantification of the in-plane shear stresses.

Appendix A. Maximum, mean, and minimum values of the measured stress values

Table 7
Maximum, mean, and minimum values of the peak Cauchy stress [kPa] measured at each stretch level for apex, body and trigone regions, see also Fig. 6.

		$\lambda = 1.1$		$\lambda = 1.2$		$\lambda = 1.3$		$\lambda = 1.4$	
		circ	long	circ	long	circ	long	circ	long
apex	max	10.92	10.14	36.24	34.23	56.77	53.88	69.09	69.15
	mean	4.59	4.74	11.47	11.99	20.18	22.16	34.14	38.53
	min	1.71	2.58	3.87	5.70	7.18	11.27	11.56	20.87
body	max	7.89	11.90	24.71	19.48	45.46	29.04	69.32	64.10
	mean	4.17	4.79	9.56	10.67	18.84	21.40	34.75	41.33
	min	2.18	2.52	5.70	6.90	12.17	13.15	21.65	23.39
trigone	max	12.25	12.95	29.55	43.14	55.36	75.21	82.04	111.34
	mean	5.22	6.04	14.64	17.40	27.82	32.62	47.53	55.73
	min	1.57	1.25	4.89	4.14	9.70	6.94	18.49	13.51

Table 8
Maximum, mean, and minimum values of the peak Cauchy stress [kPa] measured at each stretch level for ventral and dorsal regions, see also Fig. 7.

		$\lambda = 1.1$		$\lambda = 1.2$		$\lambda = 1.3$		$\lambda = 1.4$	
		circ	long	circ	long	circ	long	circ	long
ventral	max	12.25	12.95	29.55	43.14	55.36	75.21	82.04	111.34
	mean	4.18	4.94	10.69	12.68	20.02	24.40	37.12	45.04
	min	1.57	1.25	3.87	4.14	7.18	6.94	11.56	13.51
dorsal	max	10.92	11.90	36.24	34.23	56.77	54.67	69.31	88.24
	mean	5.62	5.70	14.30	14.70	26.79	27.39	42.18	45.49
	min	2.37	2.70	5.70	8.05	13.03	16.10	19.39	24.94

Appendix B. Region-specific bladder mechanical properties

Table 9
Hysteresis response sorted by region. Expansion of Table 3.

stretch	apex				body				trigone				ventral				dorsal			
ratios	circumferential		longitudinal		circumferential		longitudinal		circumferential		longitudinal		circumferential		longitudinal		circumferential		longitudinal	
λ [–]	E_{abs} [J/m^3]	E_{rel} [%]	E_{abs} [J/m^3]	E_{rel} [%]	E_{abs} [J/m^3]	E_{rel} [%]	E_{abs} [J/m^3]	E_{rel} [%]	E_{abs} [J/m^3]	E_{rel} [%]	E_{abs} [J/m^3]	E_{rel} [%]	E_{abs} [J/m^3]	E_{rel} [%]	E_{abs} [J/m^3]	E_{rel} [%]	E_{abs} [J/m^3]	E_{rel} [%]	E_{abs} [J/m^3]	E_{rel} [%]
1.1	47	50	45	49	54	49	61	48	54	43	62	43	45	46	52	46	66	51	63	47
1.2	188	54	184	55	190	54	214	53	226	49	269	48	182	52	214	53	240	53	239	51
1.3	411	57	411	57	438	55	510	55	528	51	651	51	424	55	521	55	528	54	531	52
1.4	736	57	750	57	880	56	1032	56	1044	54	1224	53	821	55	1017	56	1018	56	972	53

Table 10
Amount of shear deformation sorted by region. Expansion Table 4.

region	stretch ratios	shear deformation		shear stress	stress ratios	
	λ [–]	γ_{circ} [–]	γ_{long} [–]	σ_{shear} [kPa]	$\sigma_{shear}/_{circ}$ [%]	$\sigma_{shear}/\sigma_{long}$ [%]
apex	1.1	0.025	0.026	0.045	1.1	1.1
	1.2	0.039	0.044	0.210	2.0	1.8
	1.3	0.043	0.056	0.431	2.3	2.0
	1.4	0.054	0.068	0.846	2.8	2.2
body	1.1	0.019	0.022	0.047	1.3	1.2
	1.2	0.028	0.035	0.146	1.9	1.6
	1.3	0.040	0.045	0.342	2.1	1.8
	1.4	0.050	0.060	0.774	2.4	2.1
trigone	1.1	0.022	0.019	0.058	1.0	0.8
	1.2	0.036	0.032	0.193	1.3	1.1
	1.3	0.046	0.043	0.422	1.7	1.5

(continued on next page)

Table 10 (*continued*)

region	stretch ratios	shear deformation		shear stress	stress ratios	
	λ [–]	γ_{circ} [–]	γ_{long} [–]	σ_{shear} [kPa]	$\sigma_{shear}/_{circ}$ [%]	$\sigma_{shear}/\sigma_{long}$ [%]
	1.4	0.052	0.058	1.061	2.1	1.9
ventral	1.1	0.026	0.024	0.066	1.3	1.2
	1.2	0.042	0.036	0.230	1.6	1.5
	1.3	0.051	0.048	0.448	1.9	1.7
	1.4	0.055	0.062	0.885	2.2	1.9
dorsal	1.1	0.020	0.022	0.042	1.1	0.9
	1.2	0.031	0.037	0.159	1.7	1.5
	1.3	0.039	0.048	0.374	2.1	1.8
	1.4	0.051	0.062	0.898	2.6	2.2

Appendix C. Region-specific bladder microstructure

cients were computed. First, the degree of anisotropy (in sense of the Cauchy stress: $\sigma_{circ}/\sigma_{circ}$) for each sample location was calculated as explained in Section 3.1. Second, the projection of the fibre

Table 11
Region-specific composition of the tunica muscularis. Expansion of Table 6.

	apex			body			trigone			ventral			dorsal		
in-plane section	SM [%]	ECM [%]	fat [%]	SM [%]	ECM [%]	fat [%]	SM [%]	ECM [%]	fat [%]	SM [%]	ECM [%]	fat [%]	SM [%]	ECM [%]	fat [%]
ip1	64.5	32.2	3.2	65.0	32.5	2.5	60.6	34.2	5.2	64.3	32.4	3.4	61.6	34.2	4.1
ip2	65.3	30.4	4.3	64.9	30.9	4.1	63.3	31.7	5.0	64.5	30.9	4.6	64.6	31.2	4.2
ip3	64.5	31.9	3.6	63.1	32.2	4.7	63.5	31.6	4.8	63.3	32.4	4.3	64.6	30.9	4.5
ip4	63.4	33.1	3.5	61.7	33.9	4.4	63.8	33.4	2.8	62.1	34.3	3.6	64.6	31.8	3.6
ip5	64.2	33.1	2.7	63.0	34.5	2.5	64.1	33.6	2.2	63.0	34.6	2.5	65.4	32.1	2.5

Appendix D. Quantitative correlations between mechanical response and UB wall structure

Two qualitative relationships between region-specific mechanical response and its structure were described. In order to provide a quantitative view of these relationships, the peak stress vs. the thickness has been illustrated in Fig. 9(a) in dependence on the analysed regions. In order to calculate the stresses, peak values of all tests performed sorted by region were considered. For the thickness, all the measurement of the cross-sections sorted by region were used. It is clearly observed that body and apex regions occupy the same area of the graph indicating similar structure-response, while the trigone region appears different in both axes.

To quantify the relationship between the isotropic/anisotropic response and the fibre distribution within the bladder two coeffi-

bundles orientation on the testing axes $\boldsymbol{e}_{circ}$ and $\boldsymbol{e}_{long}$ was quantified by computing the sine and cosine of both fibre arrangements in each sample location and then, dividing the circumferential projection by the longitudinal projection, resulting in the quantity $p_{\boldsymbol{e}_{circ}}/p_{\boldsymbol{e}_{long}}$. Therefore, values lower than 1 indicate that the projection of the inner and outer fibre orientations on the testing axes is higher in the longitudinal direction while values higher than 1 indicate more circumferentially oriented. Values close to 1 means that the projections of the fibre bundles orientations on the testing axes are similar in both directions. In Fig. 9(b) the relation between $\sigma_{circ}/\sigma_{circ}$ and $p_{\boldsymbol{e}_{circ}}/p_{\boldsymbol{e}_{long}}$ is plotted in dependence on the ventral and dorsal parts. With the mean value of the 9 sample locations, we calculated a Pearson's correlation coefficient of $r = 0.796$ which indicate strong positive correlation ($r > 0.7$) [43] between the fibre bundles arrangement and the isotropic/anisotropic response.

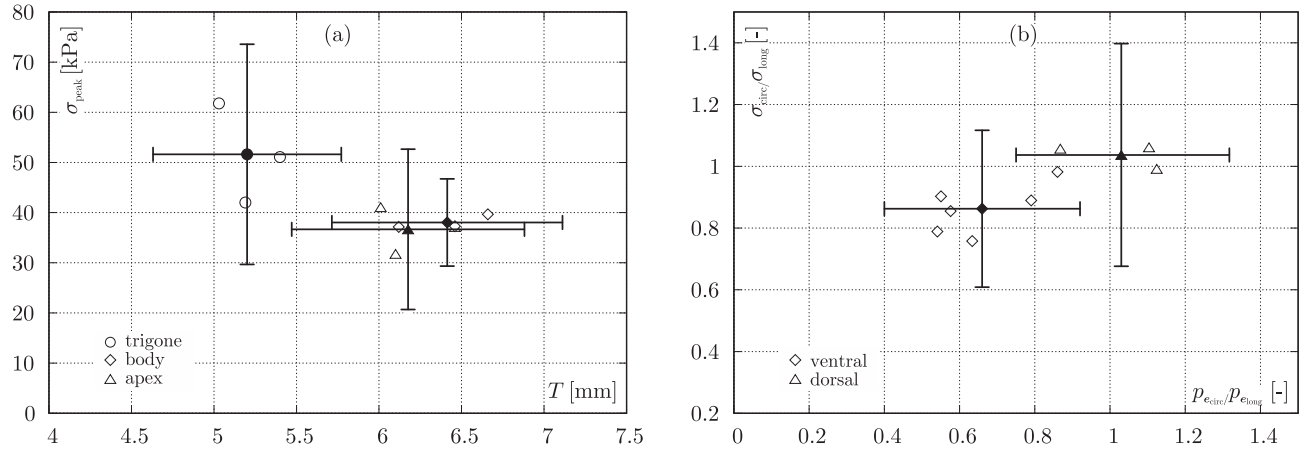

Fig. 9. Quantitative correlations between mechanical response and UB wall structure: (a) Region-specific comparison of the peak stress σ_{peak} against UB wall thickness T and (b) Correlation between fibre bundle orientation arrangements projections in terms of $p_{\boldsymbol{e}_{circ}}/p_{\boldsymbol{e}_{long}}$ and isotropic/anisotropic stress response $\sigma_{circ}/\sigma_{long}$ between ventral and dorsal parts.

Appendix E. Picro-Sirius red-staining protocol for porcine urinary bladder wall

1. Freeze the sample during 10 s in an isopentane bath cooled with liquid nitrogen.
2. Store the frozen sample wrapped in aluminum foil at −80 °C until use.
3. Cut Sections 6 μm thick at −20° C and put onto glass microscope slide.
4. Allow sections to precipitate at room temperature until the next day.
5. Fix sections with Picro-Formalin for 5 min.
6. Rinse sections under gently running water for 10 min.
7. Stain sections with Picro-Sirius red solution for 60 min.
8. Rinse sections with acidified water for 2 min 2 times.
9. Rinse sections with distilled water for 1 min.
10. Dehydrate sections with ethanol 96% for 1 min.
11. Dehydrate sections with isopropanol for 1 min 2 times.
12. Clear sections with xylene for 5 min.
13. Cover sections with a mounting medium.

Note, use some reference in the sample, e.g. dyeing one side, chamfering a corner, or puncturing the sample in a specific way, in order to align the final stained slice with the initial circumferential and longitudinal axes of the organ.

Appendix F. Elastica van Gieson staining protocol for porcine urinary bladder wall

1. Freeze the sample for 10 s in an isopentane bath cooled with liquid nitrogen.
2. Store the frozen sample wrapped in aluminum foil at −80 °C until use.
3. Cut Sections 6 micrometers thick at −20° C and place onto a glass microscope slide.
4. Allow sections to precipitate at room temperature until the next day.
5. Rinse sections with ethanol 96%, ethanol 80% and ethanol 70% for 2 min each time.
6. Stain sections with Resorcinol Fuchsine for 15 min.
7. Rinse sections under gently running water for 10 min.
8. Stain sections with Van Gieson Picrofuchsine solution for 2 min.
9. Rinse sections with distilled water for 5 s.
10. Dehydrate sections with ethanol 96% for 2 min 2 times.
11. Dehydrate sections with isopropanol for 2 min.
12. Clear sections with xylene for 5 min 2 times.
13. Cover sections with mounting medium.

References

[1] K.E. Andersson, K.D. McCloskey, Lamina propria: the functional center of the bladder?, Neurourol Urodynam. 33 (1) (2014) 9–16.
[2] S. Andersson, P. Bjerle, J. Hentschel, A. Kronström, U. Niklasson, Continuous and stepwise cystometry through suprapubic catheters – Effect of infusion pattern and infusion rate on the cystometrogram of the normal human bladder, Clin. Physiol. 9 (1) (1989) 89–96.
[3] S. Appukuttan, K.L. Brain, R. Manchanda, A computational model of urinary bladder smooth muscle syncytium, J. Comput. Neurosci. 38 (1) (2015) 167–187.
[4] R.C. Aydin, S. Brandstaeter, F.A. Braeu, M. Steigenberger, R.P. Marcus, K. Nikolaou, M. Notohamiprodjo, C.J. Cyron, Experimental characterization of the biaxial mechanical properties of porcine gastric tissue, J. Mech. Behav. Biomed. Mater. 74 (Suppl. C) (2017) 499–506.
[5] S.C. Barnes, D.E. Shepherd, D.M. Espino, R.T. Bryan, Frequency dependent viscoelastic properties of porcine bladder, J. Mech. Behav. Biomed. Mater. 42 (1) (2015) 168–176.
[6] L. Baskin, D. Meaney, A. Landsman, S.A. Zderic, E. Macarak, Bovine bladder compliance increases with normal fetal development, J. Urol. 152 (2) (1994) 692–697.
[7] M. Bayat, V. Kumar, M. Denis, J. Webb, A. Gregory, M. Mehrmohammadi, M. Cheong, D. Husmann, L. Mynderse, A. Alizad, M. Fatemi, Correlation of ultrasound bladder vibrometry assessment of bladder compliance with urodynamic study results, PLoS One 12 (6) (2017) 1–11.
[8] H.J. Benson, S.E. Gunstream, A. Talaro, K.P. Talaro, Anatomy and Physiology Laboratory Textbook: Intermediate Fetal Pig Version, William C Brown Pub., 1995.
[9] J. Bigun, T. Bigun, K. Nilsson, Recognition by symmetry derivatives and the generalized structure tensor, IEEE Trans. Pattern Anal. Mach. Intell. 26 (12) (2004) 1590–1605.
[10] M. Brandner, J. Egermaier, H. Kopincová, J. Rosenberg, Complex model of the lower urinary tract, Appl. Comput. Mech. 6 (2) (2012) 141–150.
[11] A.L. Brown, W. Farhat, P.A. Merguerian, G.J. Wilson, A.E. Khoury, K.A. Woodhouse, 22 week assessment of bladder acellular matrix as a bladder augmentation material in a porcine model, Biomaterials 23 (10) (2002) 2179–2190.
[12] S.L. Chang, J.S. Chung, M.K. Yeung, P.S. Howard, E.J. Macarak, Roles of the lamina propria and the detrusor in tension transfer during bladder filling, Scand. J. Urol. Nephrol. Suppl. 33 (201) (1999) 38–45.
[13] J. Chen, B.A. Drzewiecki, W.D. Merryman, J.C. Pope, Murine bladder wall biomechanics following partial bladder obstruction, J. Biomech. 46 (15) (2013) 2752–2755.
[14] F. Cheng, L.A. Birder, F.A. Kullmann, J. Hornsby, P.N. Watton, S. Watkins, M. Thompson, A.M. Robertson, Layer-dependent role of collagen recruitment during loading of the rat bladder wall, Biomech. Model. Mechanbiol. 17 (2) (2018) 403–417.
[15] S. Cheng, E.C. Clarke, L.E. Bilston, The effects of preconditioning strain on measured tissue properties, J. Biomech. 42 (9) (2009) 1360–1362.
[16] A.A. Claeson, V.H. Barocas, Planar biaxial extension of the lumbar facet capsular ligament reveals significant in-plane shear forces, J. Mech. Behav. Biomed. Mater. 65 (1) (2017) 127–136.
[17] B. Cruz Perez, J. Tang, H.J. Morris, J.R. Palko, X. Pan, R.T. Hart, J. Liu, Biaxial mechanical testing of posterior sclera using high-resolution ultrasound speckle tracking for strain measurements, J. Biomech. 47 (5) (2014) 1151–1156.
[18] S.E. Dahms, H.J. Piechota, R. Dahiya, T.F. Lue, E.A. Tanagho, Composition and biomechanical properties of the bladder acellular matrix graft: comparative analysis in rat, pig and human, Br. J. Urol. 82 (3) (1998) 411–419.
[19] M.S. Damaser, Whole bladder mechanics during filling, Scand. J. Urol. Nephrol. Suppl. 33 (201) (1999) 51–58.
[20] N. Dass, G. McMurray, J.E. Greenland, A.F. Brading, Morphological aspects of the female pig bladder neck and urethra: quantitative analysis using computer assisted 3-dimensional reconstructions, J. Urol. 165 (4) (2001) 1294–1299.
[21] C.M. Deveaud, E.J. Macarak, U. Kucich, D.H. Ewalt, W.R. Abrams, P.S. Howard, Molecular analysis of collagens in bladder fibrosis, J. Urol. 160 (4) (1998) 1518–1527.
[22] H. Fehervary, M. Smoljkić, J. Vander Sloten, N. Famaey, Planar biaxial testing of soft biological tissue using rakes: A critical analysis of protocol and fitting process, J. Mech. Behav. Biomed. Mater. 61 (1) (2016) 135–151.
[23] A.E. Finkbeiner, P.D. O'Donnell, Responses of detrusor smooth muscle to stretch and relaxation: in vitro study, Urology 36 (2) (1990) 193–198.
[24] A.H. Fischer, K.A. Jacobson, J. Rose, R. Zeller, Cryosectioning tissues, Cold Spring Harb Protoc 2008 (8) (2008). pdb.prot4991.
[25] D.O. Freytes, R.M. Stoner, S.F. Badylak, Uniaxial and biaxial properties of terminally sterilized porcine urinary bladder matrix scaffolds, J. Biomed. Mater. Res. 84B (2) (2008) 408–414.
[26] T.W. Gilbert, S. Wognum, E.M. Joyce, D.O. Freytes, M.S. Sacks, S.F. Badylak, Collagen fiber alignment and biaxial mechanical behavior of porcine urinary bladder derived extracellular matrix, Biomaterials 29 (36) (2008) 4775–4782.
[27] D.C. Gloeckner, Tissue biomechanics of the urinary bladder wall (Ph.D. thesis), University of Pittsburgh, Pittsburgh, PA, USA, 2003.
[28] D.C. Gloeckner, M.S. Sacks, M.O. Fraser, G.T. Somogyi, W.C. de Groat, M.B. Chancellor, Passive biaxial mechanical properties of the rat bladder wall after spinal cord injury, J. Urol. 167 (5) (2002) 2247–2252.
[29] K. Gmeiner, Ultrasonographische Charakterisierung der gesunden und kranken Harnblase bei der Sau, Universitätsbibliothek, Leipzig, 2007.
[30] J. Hornsby, Bladder Microstructural and Biomechanical Modelling: In Vivo, In Vitro and In Silico (Ph.D. thesis), Wolfson College, University of Oxford, Oxford, 2016.
[31] J. Hornsby, D.M. Daly, D. Grundy, F. Cheng, A.M. Robertson, P.N. Watton, M.S. Thompson, Quantitative multiphoton microscopy of murine urinary bladder morphology during in situ uniaxial loading, Acta Biomater. 64 (Suppl. C) (2017) 59–66.
[32] J.D. Humphrey, D.L. Vawter, R.P. Vito, Quantification of strains in biaxially tested soft tissues, J. Biomech. 20 (1) (1987) 59–65.
[33] O.P. Khanna, E.J. Barbieri, M. Altamura, R. McMichael, Vesicourethral smooth muscle: function and relation to structure, Urology 18 (2) (1981) 211–218.
[34] A.K. Kim, W.G. Hill, Effect of filling rate on cystometric parameters in young and middle aged mice, Bladder 4 (1) (2017). e28.
[35] H.E. König, H.G. Liebich, Veterinary Anatomy of Domestic Mammals: Textbook and Colour Atlas, fourth ed., Schattauer, 2009.
[36] S.M. Korogod, A.V. Kochenov, Mathematical model of the calcium-dependent chloride current in a smooth muscle cell, Neurophysiol. 45 (5) (2013) 369–378.
[37] S. Korossis, F. Bolland, J. Southgate, E. Ingham, J. Fisher, Regional biomechanical and histological characterisation of the passive porcine urinary bladder: implications for augmentation and tissue engineering strategies, Biomaterials 30 (2) (2009) 266–275.

[38] T. Lee, S.M. Yoon, The role of intra-abdominal pressure measurement in awake rat cystometry, Int. Neurourol. J. 17 (2) (2013) 44–47.
[39] D. Liao, J. Zhao, P. Kunwald, H. Gregersen, Tissue softening of guinea pig oesophagus tested by the tri-axial test machine, J. Biomech. 42 (7) (2009) 804–810.
[40] S.H. Lu, M.S. Sacks, S.Y. Chung, D.C. Gloeckner, R. Pruchnic, J. Huard, W.C. de Groat, M.B. Chancellor, Biaxial mechanical properties of muscle-derived cell seeded small intestinal submucosa for bladder wall reconstitution, Biomaterials 26 (4) (2005) 443–449.
[41] P.A. Martins, A.L. Filho, A.M. Fonseca, A. Santos, L. Santos, T. Mascarenhas, R.M. Jorge, A.J. Ferreira, Uniaxial mechanical behavior of the human female bladder, Int. Urogynecol. J. 22 (8) (2011) 991–995.
[42] R. Menzel, M. Böl, T. Siebert, Importance of contraction history on muscle force of porcine urinary bladder smooth muscle, Int. Urol. Nephrol. 49 (2) (2017) 205–214.
[43] M.M. Mukaka, A guide to appropriate use of correlation coefficient in medical research, Malawi Med. J. 24 (3) (2012) 69–71.
[44] M. Murakumo, T. Ushiki, K. Abe, K. Matsumura, Y. Shinno, T. Koyanagi, Three-dimensional arrangement of collagen and elastin fibers in the human urinary bladder: a scanning electron microscopic study, J. Urol. 154 (1) (1995) 251–256.
[45] J. Nagatomi, D.C. Gloeckner, M.B. Chancellor, W.C. deGroat, M.S. Sacks, Changes in the biaxial viscoelastic response of the urinary bladder following spinal cord injury, Ann. Biomed. Eng. 32 (10) (2004) 1409–1419.
[46] J. Nagatomi, K.K. Toosi, J.S. Grashow, M.B. Chancellor, M.S. Sacks, Quantification of bladder smooth muscle orientation in normal and spinal cord injured rats, Ann. Biomed. Eng. 33 (8) (2005) 1078–1089.
[47] J. Nagatomi, K.K. Toosi, M.B. Chancellor, M.S. Sacks, Contribution of the extracellular matrix to the viscoelastic behavior of the urinary bladder wall, Biomech. Model Mechanbiol. 7 (5) (2008) 395–404.
[48] A.N. Natali, A.L. Audenino, W. Artibani, C.G. Fontanella, E.L. Carniel, E.M. Zanetti, Bladder tissue biomechanical behavior: experimental tests and constitutive formulation, J. Biomech. 48 (12) (2015) 3088–3096.
[49] I.Z. Nenadic, B. Qiang, M.W. Urban, L.H. de Araujo Vasconcelo, A. Nabavizadeh, A. Alizad, J.F. Greenleaf, M. Fatemi, Ultrasound bladder vibrometry method for measuring viscoelasticity of the bladder wall, Phys. Med. Biol. 58 (8) (2013) 2675–2695.
[50] A. Parekh, A.D. Cigan, S. Wognum, R.L. Heise, M.B. Chancellor, M.S. Sacks, Ex vivo deformations of the urinary bladder wall during whole bladder filling: contributions of extracellular matrix and smooth muscle, J. Biomech. 43 (9) (2010) 1708–1716.
[51] D.A. Pitre, T. Ma, L.J. Wallace, J.A. Bauer, Time-dependent urinary bladder remodeling in the streptozotocin-induces diabetic rat model, Acta Diabetol. 39 (1) (2002) 23–27.
[52] K.L. Rademakers, G.A. van Koeveringe, M. Oelke, Ultrasound detrusor wall thickness measurement in combination with bladder capacity can safely detect detrusor underactivity in adult men, World J. Urol. 35 (1) (2017) 153–159.
[53] R. Rezakhaniha, A. Agianniotis, J.T. Schrauwen, A. Griffa, D. Sage, C.V. Bouten, F. N. van de Vosse, M. Unser, N. Stergiopulos, Experimental investigation of collagen waviness and orientation in the arterial adventitia using confocal laser scanning microscopy, Biomech. Model. Mechanbiol. 11 (3) (2012) 461–473.
[54] J.N. Rocha, Cystometric analysis of the transplanted bladder, Int. Braz. J. Urol. 43 (1) (2017) 112–120.
[55] D. Rohrmann, S.A. Zderic, J.W. Duckett, R.M. Levin, M.S. Damaser, Compliance of the obstructed fetal rabbit bladder, Neurourol. Urodyn. 16 (3) (1997) 179–189.
[56] A. Roosen, C. Wu, G. Sui, R.A. Chowdhury, P.M. Patel, C.H. Fry, Characteristics of spontaneous activity in the bladder trigone, Eur. Urol. 56 (2) (2009) 346–354.
[57] M.S. Sacks, A method for planar biaxial mechanical testing that includes in-plane shear, J. Biomech. Eng. 121 (5) (1999) 551–555.
[58] R. Seydewitz, R. Menzel, T. Siebert, M. Böl, Three-dimensional mechano-electrochemical model forsmooth muscle contraction of the urinary bladder, J. Mech. Behav. Biomed. Mater. 75 (1) (2017) 128–146.
[59] G. Sommer, A. Schriefl, G. Zeindlinger, A. Katzensteiner, H. Ainödhofer, A. Saxena, G.A. Holzapfel, Multiaxial mechanical response and constitutive modeling of esophageal tissues: impact on esophageal tissue engineering, Acta Biomater. 9 (12) (2013) 9379–9391.
[60] G. Sommer, D.C. Haspinger, M. Andrä, M. Sacherer, C. Viertler, P. Regitnig, G.A. Holzapfel, Quantification of shear deformations and corresponding stresses in the biaxially tested human myocardium, Ann. Biomed. Eng. 43 (10) (2015) 2334–2348.
[61] G. Sommer, A.J. Schriefl, M. Andrä, M. Sacherer, C. Viertler, H. Wolinski, G.A. Holzapfel, Biomechanical properties and microstructure of human ventricular myocardium, Acta Biomater. 24 (1) (2015) 172–192.
[62] W. Sun, M.S. Sacks, M.J. Scott, Effects of boundary conditions on the estimation of the planar biaxial mechanical properties of soft tissues, J. Biomech. Eng. 127 (4) (2005) 709–715.
[63] K. Takezawa, M. Kondo, H. Kiuchi, T. Soda, T. Takao, Y. Miyagawa, A. Tsujimura, N. Nonomura, S. Shimada, Combination of bladder ultrasonography and novel cystometry method in mice reveals rapid decrease in bladder capacity and compliance in LPS-induced cystitis, Am. J. Physiol. Renal. Physiol. 307 (2) (2014) F234–F241.
[64] K.K. Toosi, J. Nagatomi, M.B. Chancellor, M.S. Sacks, The effects of long-term spinal cord injury on mechanical properties of the rat urinary bladder, Ann. Biomed. Eng. 36 (9) (2008) 1470–1480.
[65] R. van Mastrigt, B.L. Coolsaet, W.A. van Duyl, First results of stepwise straining of the human urinary bladder and human bladder strips, Investigat. Urol. 19 (1) (1981) 58–61.
[66] C.W. Vaughan, P.M. Satchell, Urine storage mechanisms, Prog. Neurobiol. 46 (2–3) (1995) 215–237.
[67] B. Vogel, H. Siebert, U. Hofmann, S. Frantz, Determination of collagen content within picrosirius red stained paraffin-embedded tissue sections using fluorescence microscopy, MethodsX 2 (Suppl. C) (2015) 124–134.
[68] L.L. Wall, A.K. Wiskind, P.A. Taylor, Simple bladder filling with a cough stress test compared with subtracted cYstometrY for the diagnosis of urinary incontinence, Am. J. Obstet. Gynecol. 171 (6) (1994) 1472–1479.
[69] C.C. Wang, J. Nagatomi, K.K. Toosi, N. Yoshimura, J.H. Hsieh, M.B. Chancellor, M.S. Sacks, Diabetes-induced alternations in biomechanical properties of urinary bladder wall in rats, Urology 73 (4) (2009) 911–915.
[70] S. Wognum, D.E. Schmidt, M.S. Sacks, On the mechanical role of de novo synthesized elastin in the urinary bladder wall, J. Biomech. Eng. 131 (10) (2009) 101018.
[71] R.T. Woodburne, Anatomy of the bladder and bladder outlet, J. Urol. 100 (4) (1968) 474–487.
[72] E.M. Zanetti, M. Perrini, C. Bignardi, A.L. Audenino, Bladder tissue passive response to monotonic and cyclic loading, Biorheology 49 (1) (2012) 49–63.
[73] W. Zhang, Y. Feng, C.H. Lee, K.L. Billiar, M.S. Sacks, A generalized method for the analysis of planar biaxial mechanical data using tethered testing configurations, J. Biomech. Eng. 137 (6) (2015) 064501.
[74] X. Zhang, A. Alwaal, G. Lin, H. Li, U.B. Zaid, G. Wang, L. Wang, L. Banie, H. Ning, C.S. Lin, Urethral musculature and innervation in the female rat, Neurourol. Urodyn. 35 (3) (2016) 382–389.